

# A System for Simultaneous Measurement of Hysteresis Loops and Barkhausen Noise in Amorphous Ferromagnetic Ribbons

**Abstract.** This work presents a measurement system built from the ground up, allowing for the simultaneous observation of hysteresis loops and Barkhausen noise in amorphous ferromagnetic ribbons. The system consists of a solenoid that generates a uniform magnetic field and two oppositely coupled coils: a sample coil containing the magnetic material and a compensating coil. Hysteresis measurement is performed by measuring the voltage induced on the coils, which is then amplified and integrated. A hysteresis graph is a representation of calibrated magnetization values as a function of the magnetizing field.

**Streszczenie.** W niniejszej pracy przedstawiono zbudowany od podstaw układ pomiarowy pozwalający na jednoczesny pomiar pętli histerezy cienkich taśm amorficznych oraz ich szumów Barkhausena. Układ składa się z solenoizdu, który jest źródłem jednorodnego pola magnetycznego oraz dwóch cewek: pomiarowej z materiałem magnetycznym oraz kompensacyjnej połączonych przeciwsobnie. Pomiar histerezy odbywa się poprzez wzmacnianie i analogowe całkowanie sygnału napięciowego pochodzącego od strumienia magnetycznego próbki w funkcji natężenia pola magnesującego. Jedenocześnie wykonywany jest pomiar szumów Barkhausena polegający na wzmacnieniu i odfiltrowaniu sygnału o częstotliwości pola magnesującego, pochodzącego wyłącznie z cewki pomiarowej. (Układ do jednoczesnego pomiaru pętli histerezy oraz szumów Barkhausena cienkich taśm amorficznych.)

**Keywords:** magnetic hysteresis, Barkhausen noise, amorphous ribbons, measurement system

**Słowa Kluczowe:** histereza magnetyczna, szum Barkhausena, taśmy amorficzne, układ pomiarowy

## Introduction

Barkhausen noise is observed as step changes in the magnetization of ferromagnetic materials under the continuously varying intensity of an external magnetic field caused by the unstable motion of domain walls in a ferromagnetic material [1]. In thin-film amorphous materials, this process may have both statistical [2] and multifractal [3] properties. In addition to studying the movement of magnetic domains, Barkhausen noise analysis has wide applications in non-destructive material testing, such as characterizing the structure of ferromagnetic materials [4], monitoring corrosion extent [5], and evaluating stress states [6]. The nature of Barkhausen noise is also closely related to the examined ferromagnetic material's magnetic properties. Parameters such as coercivity, remanence and magnetic permeability are directly-measured from the magnetic hysteresis and are of significant importance in modeling Barkhausen noise [7]. However, there are few works in which both Barkhausen noise and hysteresis loop are measured simultaneously [8, 9]. Exploring this area may bring significant progress not only in the development of the above-mentioned methods, but also become a new area of research on the chaotic properties of Barkhausen noise. This paper present a system for simultaneous measurement of the magnetic hysteresis and Barkhausen noise, which will be the authors' next step toward researching the properties of chaotic signals [10, 11], including Barkhausen noise [12].

The presented measurement system consists of a magnetic field generator and a detector of sample magnetization. The  $H$ -field is generated by a long single-layer coil (solenoid), where the ratio  $\frac{l}{D}$  and the ratio of the sample length to its thickness are much greater than one. This geometry allows the assumption that the magnetic field  $H$  is continuous and homogeneous [13, 14]. Furthermore, using an open magnetic circuit in the experiment excludes the appearance of mechanical stresses and does not introduce additional magnetic material. As a detector for the magnetization  $M$ , two coils are used: a sample coil and a compensating coil connected oppositely [15]. Such a system ensures that the flux induced in the measuring coil, which does not originate from the sample, will be compensated. The signal from the coils is amplified and integrated and then multiplied by a calibration coefficient to obtain the  $M$  value. The magnetic hys-

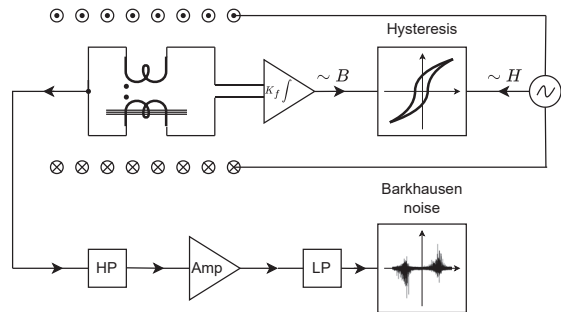


Fig. 1: The block diagram of the measuring system consists of a magnetizing coil (solenoid) and two pick-up coils oppositely coupled. The system has two measurement channels: for measuring magnetic hysteresis and Barkhausen noise.

teresis loop is obtained by plotting the dependence  $M(H)$  (on the graph given as  $\mu_0 M(H)$  in Tesla). Barkhausen noise measurement is in the same magnetic system, but the signal is acquired only from the measuring coil [16] as a voltage signal proportional to  $dB/dt$  [17]. This measurement system allows for coherent in-time observation of both the noise signal and the hysteresis loop and for placing the magnetic hysteresis parameters directly on the time series of Barkhausen noise. Thus, the evolution of the parameters describing the noise can be closely correlated with the shape of the hysteresis.

## Magnetic field calibration

Measurements of the magnetic field intensity  $H$  and the magnetization  $M$  are necessary to determine the hysteresis loop of ferromagnetic materials. In this work, it is assumed that the magnetic field standard is a single-layer air coil (solenoid), which allows for the creation of a uniform field in its interior. The intensity of this field along the axis of the solenoid can be determined using the Biot–Savart law:

$$(1) \quad H(x, \omega) = \frac{NI(\omega)}{l} \gamma(x)$$

where  $\gamma$  is a function of the position  $x$  in the following form

$$(2) \quad \gamma(x) = \left( \frac{l+2x}{2\sqrt{d^2 + (l+2x)^2}} + \frac{l-2x}{2\sqrt{d^2 + (l-2x)^2}} \right)$$

$N$  is the number of turns, and  $l$  and  $d$  are the length and diameter of the solenoid, respectively.

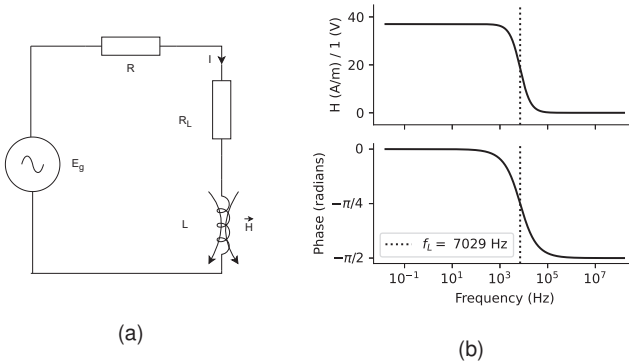


Fig. 2: The system (a) depicts the electrical circuit of the magnetic field generator, whose frequency spectrum (b) is plotted as a function of the field intensity  $H(0, \omega)$  (see Eq.(1)) per volt of the generator voltage  $E_g$  and its phase delay.

The schematic diagram of the control system for the magnetic field intensity  $H$  is shown in Fig. 2a. The current through the coil can be expressed as:

$$(3) \quad I(\omega) = \frac{E_g}{R + R_L + j\omega L}$$

where  $L$  is the inductance of the solenoid, and  $E_g$  is the voltage of generator. Substituting it into Eq.(1), the dependence of the field  $H$  on the frequency of the control voltage signal is obtained. The spectrum  $H(\omega)$  in the applied experimental system is shown in Fig. 2b. It can be observed that, due to the inductive nature of the coil, this spectrum has a cutoff frequency  $f_L = \frac{R+R_L}{2\pi L}$ , above which the inductive impedance becomes significantly greater than the coil's resistance. This situation leads to a decrease in the circuit current and, consequently, a decrease in the field intensity  $H$ . Below this frequency, the intensity is approximately constant and depends only on the voltage value of the source  $E_g$ . In the middle of the solenoid, it satisfies:

$$(4) \quad H \approx \alpha E_g$$

where  $\alpha = \frac{N}{\sqrt{l^2+d^2}} \frac{1}{R+R_L}$  is a proportionality coefficient containing parameters related to the coil geometry and the electric circuit.

The solenoid used in the experiment has 458 turns, a length of 243.5 mm, and a diameter of 36.8 mm. The measured series resistance ( $R + R_L$ ) is  $50.8 \Omega$ , and the coil inductance is  $1.083 \text{ mH}$ . The calibration parameter  $\alpha$  is  $36.6 \text{ A}/(\text{m}\cdot\text{V})$  (with a standard uncertainty of 0.9, see Tab.1), and the limit frequency  $f_L$  is 7029 Hz (see Fig. 2b). Magnetic hysteresis is typically measured at frequencies ranging from 1 Hz to 100 Hz, which is at least an order of magnitude lower than the cutoff frequency  $f_L$ . Such a system can, therefore, be used as a simple magnetic field standard linearly dependent on the control voltage. More accurate calibration is possible using a more precise H-field measurement device.

### Magnetization calibration

Placing a sample of ferromagnetic material in the area of a uniform magnetic field (inside the solenoid) induces a secondary field resulting from the organizing dipole moments of the ferromagnetic material. The total magnetic field is equal to the sum of the field generated by the solenoid and the sample magnetization field  $M$ . This field can be measured using a pick-up coil surrounding the sample.

In the experimental system proposed by the authors, this measurement is carried out by two series-connected coils inside the solenoid with diameter 10.4 mm and inductance  $714 \mu\text{H}$ , arranged parallel to each other and the lines of the magnetic field. The first pick-up coil contains the ferromagnetic sample, while the second coil (compensating) is empty. The electromotive force induced by the magnetic fluxes coming from the solenoid and the sample can be written as:

$$(5) \quad \begin{aligned} E &= j\omega\phi_1 \pm j\omega\phi_2 \\ &= j\omega(\phi_{h1} + \phi_m) \pm j\omega\phi_{h2} \\ &= j\omega\phi_{h1} \pm j\omega\phi_{h2} + j\omega\phi_m \end{aligned}$$

Depending on the type of coil coupling, the voltages induced in the pick-up coils coming from the solenoid's magnetic field may be in-phase (cumulatively coupled) or anti-phase (oppositely coupled). Therefore, if the coils are oppositely coupled ( $-j\omega\phi_{h2}$ ) and the induced fluxes are identical ( $\phi_{h1} = \phi_{h2}$ ), the output voltage takes the form:

$$(6) \quad E_p = j\omega\phi_m = j\omega n_1 \mu_0 M s_p$$

where  $s_p$  is the cross-section of the sample and  $n_1$  is the number of turns of the pick-up coil.

From the equation (6) it follows that the induced voltage is directly proportional to the derivative of the magnetization ( $j\omega M$ ), therefore to measure  $M$  an integrating circuit is necessary. In general, it can be assumed that the magnetic flux detector system (comprising the pick-up coils and the amplifying-integrating circuit) should be a linear flux-to-voltage converter system that satisfies the equation:

$$(7) \quad V_{out} = K_f \Phi$$

where  $K_f$  is the linear conversion coefficient. This coefficient can be empirically determined in the proposed measurement system for cumulatively coupled pick-up coils without sample. The total flux is then equal to:

$$(8) \quad \Phi = \phi_{h1} + \phi_{h2} = n_1 \mu_0 H s_1 + n_2 \mu_0 H s_2$$

If the coils are identical, the above relationship can be expressed using equation (4) as follows:

$$(9) \quad \Phi \approx 2n\mu_0 H s = 2n\mu_0 \alpha E_g s$$

The error associated with this approximation has been minimized by empirically adjusting the compensating pick-up coil so that the relative error of the voltage difference between both coils is below 1%. From (9) it can be seen that the total flux  $\Phi$  is proportional to the control voltage  $E_g$ . To calibrate the system it is necessary to measure the output voltage  $V_{out}$  as a function of the generator voltage  $E_g$ . The ratio of these voltages should be constant and satisfy the following equation:

$$(10) \quad V_{out} = m E_g$$

where  $m$  is the proportionality coefficient. To find the relationship between  $K_f$  and  $m$ , the total magnetic flux from the equation (9) must be substituted into the (7), then the voltage at the detector output can be written as:

$$(11) \quad V_{out} = K_f 2n\mu_0 \alpha E_g s$$

Finally, the coefficient  $K_f$  is obtained by equating the both sides of the (11) and (10):

$$(12) \quad K_f = \frac{m}{\mu_0 \alpha s 2n}$$

The sample magnetization can be determined by substituting the magnetic flux  $\phi_m$  from the equation (6) and the rated coefficient  $K_f$  from the equation (12) into the equation for the detector output voltage (7), obtaining:

$$(13) \quad M = 2 \frac{\alpha}{m s_p} \frac{s}{V_{out}}$$

Similarly to the case of the H-field calibration, the M-field is linearly dependent on the voltage  $E_g$ , and its value depends on several coefficients that are obtained empirically. Thus, the primary origin of errors in determining magnetization will be the measurement of parameters related to the geometry of the coils ( $\alpha$  and  $s$ ), the electrical gauging of the magnetic system ( $m$ ), and the cross-sectional area of the sample ( $s_p$ ). Ultimately, this equation can be simplified to:

$$(14) \quad M = \beta V_{out}$$

where  $\beta$  is the calibration coefficient:

$$(15) \quad \beta = 2\mu_0 \frac{\alpha}{m s_p} \frac{s}{V_{out}}$$

### Electrical circuit of the magnetic hysteresis measurement system

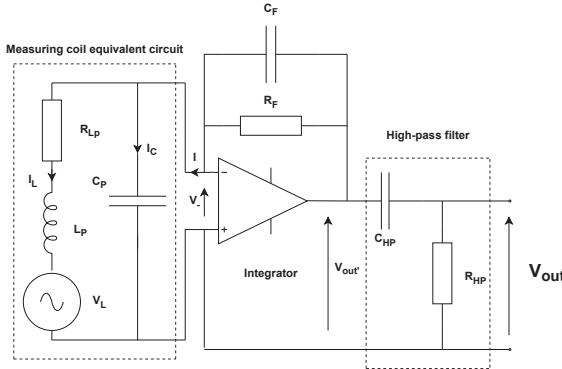


Fig. 3: Scheme of the system for measuring the magnitude of the magnetization vector. The system consists of an equivalent circuit of oppositely coupled coils, an integrating amplifier, and a low-pass filter. The output voltage is proportional to  $M$ .

The electrical part of the magnetization measurement system was shown in Fig. 3. The oppositely coupled coils were replaced by a common equivalent circuit consisting of an ideal coil  $L_p$ , series resistance  $R_{Lp}$ , and equivalent capacitance  $C_p$ . The induced magnetic flux is presented in the diagram as a voltage source with the value:

$$(16) \quad V_L = j\omega\Phi$$

The output current of the coil in the equivalent circuit used contains two components:

$$(17) \quad I = I_L + I_C$$

where  $I_L$  is the current flowing through the equivalent inductance, which can be described by the equation:

$$(18) \quad I_L = \frac{V_- - V_L}{j\omega L_p + R_{Lp}}$$

and  $I_C$  which is the current of the equivalent capacitance, expressed by the equation:

$$(19) \quad I_C = V_- j\omega C_p$$

The integrating amplifier can be described by the following system of equations:

$$(20) \quad \begin{cases} I = \frac{V_{out'} - V_-}{R_f || C_f} \\ V_{out'} = A(\omega)V_- \end{cases}$$

where  $A(\omega)$  is the open-loop amplifier gain:

$$(21) \quad A(\omega) = \frac{A_0}{1 + j\frac{\omega}{\omega_0}}$$

Converting the equations from (17) to (20) the final form is obtained:

$$(22) \quad \begin{aligned} V_{out'} &= \frac{j\omega\Phi}{\frac{1+A(\omega)\Gamma(\omega)}{A(\omega)\Gamma(\omega)} \frac{(R_{Lp}+j\omega L_p)(1+j\omega R_f C_f)}{R_f} + \frac{1}{A(\omega)}} \\ \Gamma(\omega) &= \frac{1}{1 + \frac{j\omega R_f C_p}{1+j\omega R_f C_f}} \end{aligned}$$

The detector system additionally has a final high-pass filter that cuts off the offset voltage of the integrating amplifier. Ultimately, the output voltage of the system takes the form:

$$(23) \quad V_{out} = \frac{1}{1 + \frac{1}{j\omega C_{HP} R_{HP}}} V_{out'}$$

The gain in a given frequency band is:

$$(24) \quad V_{out} \approx \frac{j\omega\Phi}{j\omega R_{Lp} C_f + \frac{j\omega}{A_0 \omega_0}}$$

It will be true if the following conditions are met:

$$(25) \quad \omega \gg \omega_0 \wedge \omega \gg \frac{1}{R_f C_f} \wedge \omega \ll \frac{R_{Lp}}{L_p} \wedge \omega \gg \frac{1}{C_{HP} R_{HP}}$$

and the coil capacitance  $C_p$  will be negligible ( $\Gamma \approx 1$ ).

Such a system satisfies the conditions of the equation (7), and the linear conversion factor of flux-to-voltage will be:

$$(26) \quad K_f = \frac{1}{R_{Lp} C_f + \frac{1}{A_0 \omega_0}}$$

This property of the measurement system allows it to be designed such that the bandwidth and gain are matched to the dynamics of the measured signal. On the other hand, none of these parameters enter into the uncertainty calculation because  $K_f$  can be determined experimentally as shown in equation (12).

### Barkhausen noise measurement system

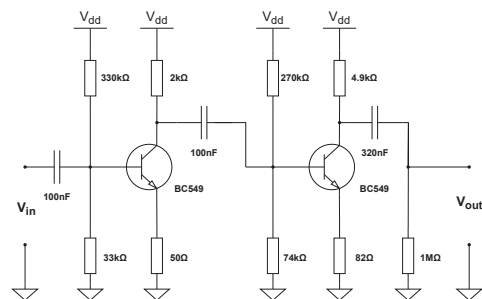


Fig. 4: Selective amplifier circuit for measuring Barkhausen noise. The amplifier consists of a two-stage common emitter system, which has a gain of approximately 60 dB in the band 500 Hz to 100 kHz.

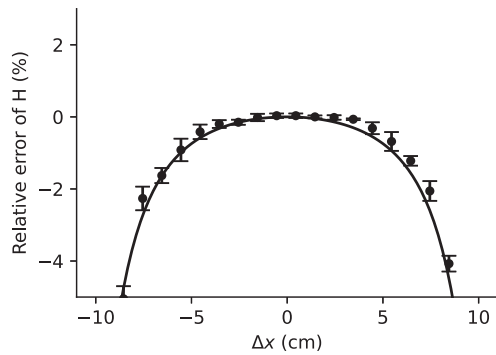


Fig. 5: Measurement of the uniformity of the magnetic field intensity inside the coil as a function of the position relative to the center of the coil. The points and uncertainties represent the relative error ( $\Delta H/H(x=0)$ ). The theoretical field (see Eq.(1)) distribution is marked with a solid line.

The system for measuring Barkhausen noise consists of a selective amplifier built using a two-stage transistor circuit with a common emitter (see Fig. 4). The amplifier's bandwidth ranges from 500 Hz to 100 kHz, with a gain of approximately 60 dB. This system also acts as a low-pass filter, removing the frequency  $f_0$  and amplifying the noise signal as shown in Fig. 1. The noise measurement is performed by observing the signal as a function of time [11].

#### Testing and calibration of magnetic hysteresis measurement system

This chapter is dedicated to testing and calibration the system for magnetic hysteresis measurement. First, the uniformity of the magnetic field intensity along the solenoid axis was measured. The results are presented in Fig. 5. The solid line marks the relative error of the field intensity to the value in the center of the coil ( $\Delta H/H(x=0)$ ), determined using (1). The points with uncertainties represent the measurements performed. The obtained relative error is below 1% for distances of  $\pm 7$  cm. It means that the resulting field gradient in this area is negligible, and it can be assumed that the field along the tested sample is uniform.

Secondly, the impedance of the pick-up coils was measured in the equivalent circuit as shown in Fig. 3. The measurement involved determining the effective current and voltage values for different input signal frequencies on the coils. The inductance and equivalent capacitance were determined using linear regression on the measurement data, while the series resistance value was obtained through DC measurements. The following results were obtained:

$$(27) \quad \begin{aligned} L_p &= (737.0 \pm 0.8)\mu H \\ C_p &= (33.3 \pm 0.1)pF \\ R_p &= (6.7 \pm 0.2)\Omega \end{aligned}$$

If the equivalent capacitance  $C_p$  is much smaller than the capacitance of the integrating capacitor  $C_F$  (see Fig. 3), then the factor  $\Gamma(\omega)$  in the equation (22) becomes negligible.

Finally, spectral measurements of the detection system were also performed, and the magnetization calibration coefficient was determined. The first step was to determine the ratio between the output voltage from the detector ( $V_{out}$ ) and the control voltage ( $E_g$ ) in the frequency range from 1 Hz to 100 MHz. The measurement results are presented in the form of a frequency response chart (Fig. 6a) and phase characteristics (Fig. 6b). The figure's solid line represents the

theoretical function of  $K_f(\omega)$ , determined based on equation (22). The dashed line shows the spectrum of the system containing a sample with high magnetic permeability (the inductance of the pick-up coils with the sample is about 1.7 mH). The points in Figure Fig. 6 represent the measurement results for the system without the sample and with the cumulatively coupled coils. A -3 dB bandwidth from about 1 Hz to 4.5 kHz was obtained.

To determine the calibration coefficient  $\beta$  (see (15)), it was necessary to measure the parameter  $m$  (see (10)). This measurement determines the ratio  $V_{out}/E_g$  for the frequency for which the phase shift is zero. Using the phase characteristics (see Fig. 6b), it was found that this frequency is approximately 60 Hz. The parameter  $m$  was determined on the basis of a measure of  $V_{out}(E_g)$  characteristics for a sinusoidal signal with a frequency of 60Hz. Using the linear regression method, the slope of the straight line was obtained, as shown in Fig. 6b. The regression error is very small (relative error at  $10^{-5}$ ), and linearity is maintained throughout the examined dynamic range. Taking into account the sample dimensions and the diameters of the measuring coil, we can determine the cross-sections  $s_p = 0.21mm^2$  and  $s = 85mm^2$ . Finally, the beta coefficient is equal  $\beta = 129.1 A/(m\cdot mV)$ .

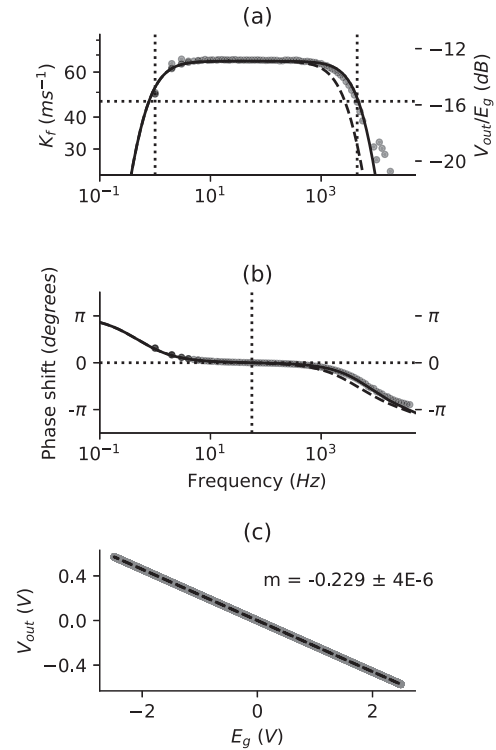


Fig. 6: Figure (a) presents the spectral characteristic and (b) the phase characteristic of the parameter  $K_f$ . The spectra were determined using equation Eq.26 for the coil without the sample (solid line) and with the sample (dashed line). The measurements of the function  $m(\omega)$  were marked with points. Figure (c) shows the measurement of the parameter  $m$  for the center frequency  $f_0 = 60Hz$ .

#### Exemplary results

This chapter presents an example of three amorphous ribbons measurement (iron-boron alloys with various dopants), each approximately 50 mm long, 3.5 mm wide, and about 60  $\mu m$  thick. Ribbons were successively placed in the pick-up coil and then magnetized with a variable magnetic

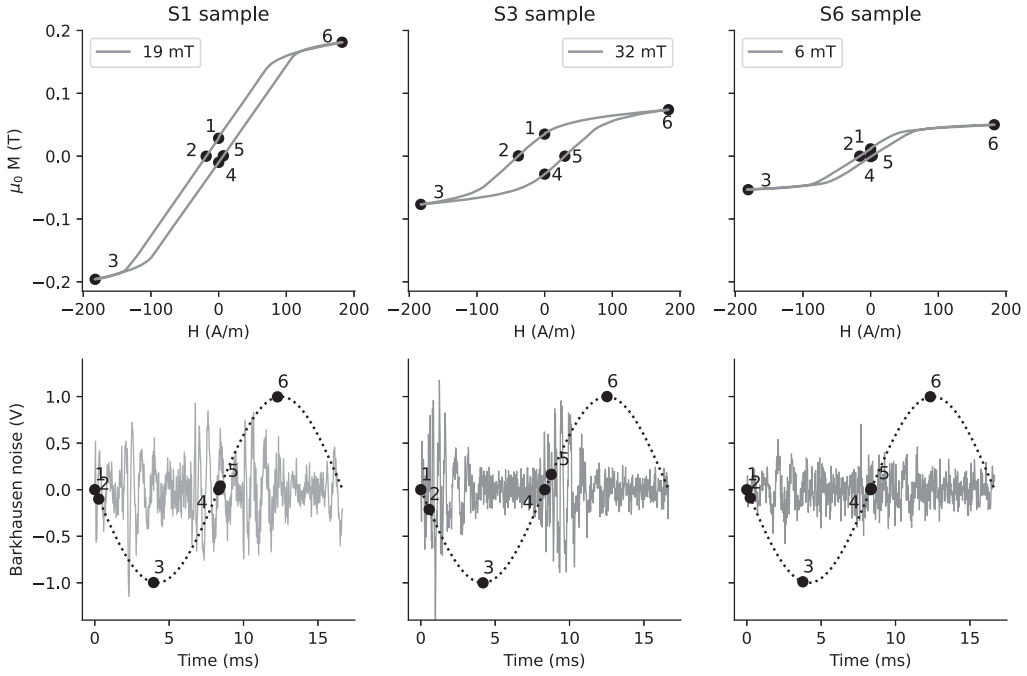


Fig. 7: The graphs present the magnetic measurements of three amorphous ribbons. The upper plots show the hysteresis loop measurements for different magnetic field intensities, corresponding to three different remanence values  $M_R$ . The lower plots represent the Barkhausen noise measurements made simultaneously with the hysteresis measurements. The points on the graphs represent characteristic values for the hysteresis loops and have been correspondingly transferred to the time course of the Barkhausen noise.

field at the frequency of 60 Hz and field intensities of 183 A/m. The results were shown in Fig. 7. The top row shows the  $M(H)$  dependencies, which form hysteresis loops for ferromagnets. Samples S1 and S3 have low coercive fields, and sample S1 has a high saturation compared to the others. The bottom row presents the time courses of Barkhausen noise for the respective samples and magnetizing field intensities.

In the hysteresis loop plots, six characteristic points are marked, numbered from 1 to 6. Points 2 and 5 represent the situations where  $M(H) = 0$ , and half the distance between these points is called the coercive field  $H_c$ . Points 1 and 4 correspond to the situation where the magnetizing field vanishes ( $M(0)$ ) and represents the state of permanent magnetization of the sample, known as remanence  $M_R$ . Points 3 and 6 are the extreme points where the magnetizing field intensity reaches its maximum. These points are reflected in the time courses of Barkhausen noise. It can be observed that the noise achieves its peak amplitude between points 1-2 and 4-5. A detailed analysis of the obtained results will be the main topic of the authors' following paper.

### Uncertainties

This chapter will discuss the uncertainties in determining the magnetic quantities  $M$  and  $H$  using the presented measurement system. According to equation (4), the magnetic field intensity will have two components of uncertainty. The first is the parameter  $\alpha$ , which includes quantities related to the coil's geometry and resistance. The combined uncertainty of this parameter can be expressed as follows:

$$(28) \quad u(\alpha) = \sqrt{\left(\frac{\partial \alpha}{\partial N}\right)^2 u^2(N) + \left(\frac{\partial \alpha}{\partial l}\right)^2 u^2(l) + \left(\frac{\partial \alpha}{\partial d}\right)^2 u^2(d) + \left(\frac{\partial \alpha}{\partial(R+R_L)}\right)^2 u^2(R+R_L)}$$

The values of the individual components and the total combined uncertainty are presented in Table 1. It can be observed that the uncertainty of determining  $\alpha$  is mainly influenced by measuring the resistance. Ultimately, the uncertainty in scaling the magnetic field intensity with the voltage on the generator will be equal to:

$$(29) \quad u(H) = \left| \frac{\partial H}{\partial \alpha} u(\alpha) \right| = E_g u(\alpha)$$

The uncertainty of the magnetization determination also consists of two components: the coefficient  $\beta$  and the control voltage  $E_g$ . The uncertainty of the first component can be determined from (15) as follows:

$$(30) \quad u(\beta) = \sqrt{u^2(\beta) = \left(\frac{\partial \beta}{\partial \alpha}\right)^2 u^2(\alpha) + \left(\frac{\partial \beta}{\partial m}\right)^2 u^2(m) + \left(\frac{\partial \beta}{\partial s}\right)^2 u^2(s) + \left(\frac{\partial \beta}{\partial s_p}\right)^2 u^2(s_p)}$$

Similarly to the previous case, the results for the individual components and the total combined uncertainty are presented in Table 1. The determining factor for measurement uncertainty is, once again, the measurement of the coil resistance, which significantly affects the dominant component – the parameter  $\alpha$ . Ultimately, the uncertainty in the magnetization measurement can be expressed by the equation:

$$(31) \quad u(M) = \left| \frac{\partial M}{\partial \beta} u(\beta) \right| = V_{out} u(\beta)$$

### Conclusion

This paper presents a system for the simultaneous measurement of hysteresis loops and Barkhausen noise, as well

Table 1: Values of individual components of the combined uncertainty of the  $\alpha$  and  $\beta$  parameters along with their total values.

$x_n$	Relative error (%)	$\frac{\partial \alpha}{\partial x_n} u(x_n)$
$N$	10.9	4.0E-1
$l$	0.1	3.9E-2
$d$	0.5	5.9E-1
$R + R_L$	17.8	6.6E-1
$\alpha$	<b>20.8</b>	<b>8.7E-1</b>
$x_n$	Relative error (%)	$\frac{\partial \beta}{\partial x_n} u(x_n)$
$\alpha$	23.5	3.4E-3
$m$	0.01	2.9E-6
$s$	3.8	6.3E-4
$s_p$	5.7	9.4e-4
$\beta$	<b>21.9</b>	<b>4.0E-3</b>

as its metrological analysis. The system used an open magnetic circuit, allowing for the observation of signals originating from domain walls located in the area of the measuring coil. There are two ways to close a magnetic circuit. The first method is introducing a magnetic lock made of a soft magnetic material into the circuit. The second method consists of making a toroidal circuit from the tested material. In both cases, there may be a change in the dynamics of the domain walls, affecting the measured correlation dimension of the magnetization signal.

The proposed measurement system is characterized by high uniformity of the magnetic field and ease of determining its value, which is particularly important in Barkhausen noise studies. Using oppositely coupled coils, ensures that the error in magnetization measurement largely depends on the error in determining the magnetizing field. The measuring system is also sensitive to phase shifts when determining the hysteresis loop. Small deviations from the center frequency of the detector system cause phase delays between the measured H-field and the M-field. In addition, introducing a sample with high magnetic permeability can also cause small phase errors resulting from the change of the upper cut-off frequency. These errors can be minimized by broadening the transmission band of the measuring system. Changing the magnetization frequency, however, may require redesigning the detector system. Moreover, considering the fact that Barkhausen noise measurements can be performed in a wide range of these frequencies, this may prove to be particularly troublesome. In the system proposed by the authors, the magnetization frequency is in the order of tens of hertz, which creates the possibility of measuring noise with the highest amplitude [18].

Measurements of Barkhausen noise characteristics are crucial for understanding their nature. This noise can exhibit deterministic chaos or stochastic behavior. One of the goals of Barkhausen noise research is to establish the relationship between the shape of the hysteresis loop and the correlation dimension of the noise. Also, the discussed magnetization frequency may have a significant influence on the dimension value. The presented system satisfies the requirements for accurately determining the correlation dimension by minimizing the area of Barkhausen signal collection. We have yet to find similar solutions in the literature. Errors in determining the correlation dimension of chaotic signals are influenced by the methods of signal acquisition representing the studied dynamic system and subsequent processing, as described in the paper [11]. In summary, the presented system will enable

further research into the nature of the magnetization dynamics of magnetic materials.

**Authors:** MSc Karol Bolek, email: karol.bolek@pw.edu.pl, Prof. Michał K. Urbański, Faculty of Physics, Warsaw University of Technology, Koszykowa 75, 00-662 Warsaw, Poland

## REFERENCES

- [1] G. Durin and S. Zapperi, "Chapter 3 - The Barkhausen Effect," in *The Science of Hysteresis* (G. Bertotti and I. D. Mayergoyz, eds.), pp. 181–267, Oxford: Academic Press, 2006.
- [2] F. Bohn, M. A. Corrêa, M. Carara, S. Papanikolaou, G. Durin, and R. L. Sommer, "Statistical properties of Barkhausen noise in amorphous ferromagnetic films," *Physical Review E*, vol. 90, p. 032821, Sept. 2014.
- [3] G. Z. Dos Santos Lima, M. A. Corrêa, R. L. Sommer, and F. Bohn, "Multifractality in domain wall dynamics of a ferromagnetic film," *Physical Review E*, vol. 86, p. 066117, Dec. 2012.
- [4] D. Mascareñas, M. Lockhart, and T. Lienert, "Barkhausen noise as an intrinsic fingerprint for ferromagnetic components," *Smart Materials and Structures*, vol. 28, p. 015014, Jan. 2019.
- [5] M. Neslušan, F. Bahleda, P. Minárik, K. Zgútová, and M. Jambor, "Non-destructive monitoring of corrosion extent in steel rope wires via Barkhausen noise emission," *Journal of Magnetism and Magnetic Materials*, vol. 484, pp. 179–187, Aug. 2019.
- [6] T. Garstka, "An attempt of characterization of stress state in high carbon C68D steel wire rod by Barkhausen noise method," *PRZEGŁĄD ELEKTROTECHNICZNY*, vol. 1, pp. 22–25, Apr. 2015.
- [7] D. C. Jiles and W. Kiarie, "An Integrated Model of Magnetic Hysteresis, the Magnetomechanical Effect, and the Barkhausen Effect," *IEEE Transactions on Magnetics*, vol. 57, pp. 1–11, Feb. 2021.
- [8] M. M. Sawalem and M. M. Blaow, "Evaluation of Residual Stresses in Grinding by Magnetic Barkhausen Noise," vol. 2, no. 2, 2016.
- [9] N. J. Weigman, "Barkhausen effect in magnetic thin films: Experimental noise spectra," *Applied Physics*, vol. 12, pp. 157–161, Feb. 1977.
- [10] K. Bolek and M. K. Urbański, "Influence of Measuring System Noise on the Fractal Dimension of the Chaotic Signal Attractor," *PRZEGŁĄD ELEKTROTECHNICZNY*, vol. 1, pp. 70–73, Dec. 2022.
- [11] K. Bolek and M. K. Urbański, "Effect of the Preamplifier Stage on the Acquisition of Low-Amplitude Nonlinear Dynamics Signals," *PRZEGŁĄD ELEKTROTECHNICZNY*, vol. 99, no. 10, pp. 200–203, 2023.
- [12] P. Plewka, J. J. Żebrowski, and M. Urbański, "Determinism and correlation dimension of Barkhausen noise," *Physical Review E*, vol. 57, pp. 6422–6431, June 1998.
- [13] E. E. Callaghan and S. H. Maslen, "The magnetic field of a finite solenoid," *NASA Technical Reports*, Oct. 1960.
- [14] A. P. Golovitskii and A. V. Pelli, "Calculations of the parameters of the single-layer solenoidal inductor of finite length surrounded by a lossy dielectric medium," *Journal of Communications Technology and Electronics*, vol. 62, pp. 838–848, Aug. 2017.
- [15] S. Tumanski, "Modern magnetic field sensors – a review," *PRZEGŁĄD ELEKTROTECHNICZNY*, vol. 89, no. 10, pp. 1–12, 2013.
- [16] S. Santa-aho, A. Laitinen, A. Sorsa, and M. Vippola, "Barkhausen Noise Probes and Modelling: A Review," *Journal of Nondestructive Evaluation*, vol. 38, p. 94, Dec. 2019.
- [17] O. Ortega-Labra, P. Martínez-Ortíz, T. L. Manh, E. Velazquez-Lozada, and J. Pérez-Benítez, "What does a Barkhausen surface coil actually measure ?," *Journal of Magnetism and Magnetic Materials*, vol. 563, p. 169938, Dec. 2022.
- [18] M. Neslušan, K. Zgútová, M. Pitoňák, and D. Kajánek, "Influence of Magnetizing Conditions on Barkhausen Noise in Fe Soft Magnetic Materials after Thermo-Mechanical Treatment," *Materials*, vol. 15, p. 7239, Oct. 2022.